Title
Niche-Specific Factors Dynamically Regulate Sebaceous Gland Stem Cells in the Skin.

Journal
Developmental cell, 51(3)

ISSN
1534-5807

Authors
Veniaminova, Natalia A
Grachtchouk, Marina
Doane, Owen J
et al.

Publication Date
2019-11-01

DOI
10.1016/j.devcel.2019.08.015

Peer reviewed

HHS Public Access

Author manuscript

Dev Cell. Author manuscript; available in PMC 2020 November 04.

Published in final edited form as:

Dev Cell. 2019 November 04; 51(3): 326–340.e4. doi:10.1016/j.devcel.2019.08.015.

Niche-specific factors dynamically regulate sebaceous gland stem cells in the skin

Natalia A. Veniaminova[1], **Marina Grachtchouk**[1], **Owen J. Doane**[1], **Jamie K. Peterson**[1], **David A. Quigley**[2], **Madison V. Lull**[1], **Daryna V. Pyrozhenko**[1], **Raji R. Nair**[1], **Matthew T. Patrick**[1,3], **Allan Balmain**[2], **Andrzej A. Dlugosz**[1], **Lam C. Tsoi**[1,3], **Sunny Y. Wong**[1,*]

[1]Departments of Dermatology and Cell and Developmental Biology, University of Michigan, Ann Arbor, MI 48109

[2]Helen Diller Family Comprehensive Cancer Center, UCSF, San Francisco, CA 94158

[3]Department of Computational Medicine & Bioinformatics; Department of Biostatistics, University of Michigan, Ann Arbor, MI 48109

Summary

Oil-secreting sebaceous glands (SGs) are critical for proper skin function; however, it remains unclear how different factors act together to modulate SG stem cells. Here, we provide functional evidence that each SG lobe is serviced by its own dedicated stem cell population. Upon ablating Notch signaling in different skin subcompartments, we find that this pathway exerts dual counteracting effects on SGs. Suppressing Notch in SG progenitors traps them in a hybrid state where stem and differentiation features become intermingled. In contrast, ablating Notch outside of the SG stem cell compartment indirectly drives SG expansion. Finally, we report that a K14:K5→K14:K79 keratin shift occurs during SG differentiation. Deleting K79 destabilizes K14 in sebocytes, and attenuates SGs and eyelid Meibomian glands, leading to corneal ulceration. Altogether, our findings demonstrate that SGs integrate diverse signals from different niches, and suggest that mutations incurred within one stem cell compartment can indirectly influence another.

eTOC

Sebaceous glands secrete oils that moisturize and protect the skin. Veniaminova et al., show that sebaceous gland stem cells are both directly and indirectly regulated by Notch signaling. Furthermore, they show that proper maintenance of these glands in the skin and eyelid depends upon Keratin 79.

*Corresponding Author and Lead Contact: sunnyw@umich.edu.

Author Contributions

Conceptualization and methodology, N.A.V. M.G., A.A.D., L.C.T. and S.Y.W.; Investigation, N.A.V., O.J.D., J.K.P., M.V.L., D.V.P., R.N.; Formal Analysis, D.A.Q., M.T.P., A.B., L.C.T.; Writing – Original Draft, Review & Editing: N.A.V., S.Y.W.; Funding Acquisition and Supervision, S.Y.W.

Declaration of Interests

The authors declare no competing interests.

Keywords

sebaceous glands; hair follicles; skin biology; epithelial stem cells; K79; Krt79

Introduction

Our skin acts as a protective barrier that shields us from our environment while serving as an interface for gas and liquid exchange. This barrier is formed as keratinocytes detach from the basement membrane and initiate terminal differentiation, undergoing a specialized form of cell death known as cornification (Candi et al., 2005; Doupe and Jones, 2012). As cornifying cells rise up through the stratified layers of the epidermis, their remains become incorporated into an insoluble protein network embedded within a lipid matrix. This structure constitutes a physical barrier that is pliable but rigid, selectively permeable, and essential for life (Hardman et al., 1998).

Proper skin function depends upon sebaceous glands (SGs), which are comprised of differentiated sebocytes that release oils onto the skin's surface (Niemann and Horsley, 2012; Schneider and Paus, 2010; Zouboulis et al., 2016). Although the evolutionary origins for SGs are murky, these acinar epithelial appendages may have arisen in early tetrapods to facilitate their adaptation from aquatic to terrestrial life (Stenn et al., 2008). Indeed, by some estimates SGs may contribute up to 90% of the lipids in the epidermis. These lipids, which are secreted as part of a complex mixture known as sebum, are thought to serve numerous roles, including skin hydration, water repulsion, thermoregulation, as well as anti-oxidant and anti-microbial functions (Dahlhoff et al., 2016; Ehrmann and Schneider, 2016; Kobayashi et al., 2019; Zhang et al., 2014). Conversely, defective SGs have been linked to a variety of skin disorders including acne, seborrheic dermatitis, eczematous diseases, psoriasis and cicatricial alopecia (Karnik et al., 2009; Lovászi et al., 2017; Rittié et al., 2016; Shi et al., 2015; Smith and Thiboutot, 2008).

SGs are typically associated with hair follicles, although specialized SGs can also arise independently at sites such as the eyelid, where they are known as Meibomian glands (Ehrmann and Schneider, 2016). In mice, lineage tracing studies have suggested that hair follicle-associated SGs are maintained by resident stem cell populations found along the periphery of these glands (Füllgrabe et al., 2015; Ghazizadeh and Taichman, 2001; Jensen et al., 2009; Page et al., 2013). As these progenitors differentiate into sebocytes, they enter the gland's interior, accumulate lipids and eventually burst, releasing their contents into the sebaceous duct (Schneider and Paus, 2010) (Figure 1A).

The regulation of SGs is complex and likely mediated both by local and long-range signals, including hormones. Although numerous mouse mutants have been reported to possess SG defects (Ehrmann and Schneider, 2016), in many cases it remains unclear whether these phenotypes are caused by a direct effect on SG stem cells, or are an indirect consequence of generalized skin defects. Indeed, while the different domains of the skin and hair follicle are compartmentalized and replenished by independent stem cell populations (Schepeler et al., 2014), emerging evidence also suggests that there is likely extensive bi-directional communication among these populations, as well as with their differentiated progeny.

Untangling these signals is key to understanding how the different sub-structures in our skin respond to changes within our body, as well as to challenges from the environment.

As we age, our skin also changes. Barrier function becomes compromised, hair grows less frequently, and SGs expand but secrete less sebum (Matsumura et al., 2016; Rittié and Fisher, 2015; Zouboulis and Boschnakow, 2001). Some of these effects may be attributable to stem cell exhaustion and alterations in the dermis. At the same time, aged, sun-exposed skin harbors the highest mutational burden of any organ in the body (Martincorena et al., 2015), which may accelerate aging-associated changes over time. Among the most common mutations are those which occur within the Notch pathway, a central mediator of epithelial differentiation (Lynch et al., 2017; Martincorena et al., 2015; Nowell and Radtke, 2013; Watt et al., 2008). Although previous studies have reported that Notch-deficient mice possess severe skin developmental defects, including aberrant SGs, the generalized nature of these defects obscures Notch's specific role in modulating SG stem cells (Blanpain et al., 2006; Demehri et al., 2009a; Dumortier et al., 2010; Pan et al., 2004; Rangarajan et al., 2001; Vauclair et al., 2005; Weber et al., 2011). In addition, it remains unclear whether Notch mutations incurred during adulthood affect skin homeostasis and aging.

In this study, we show that SG stem cells are exquisitely sensitive to multiple overlapping, and often contradictory, cues that arise both locally and from a distance. In particular, we demonstrate that a single pathway, Notch, can simultaneously manifest diametrically opposed effects on SGs. In this way, SGs behave as adaptable mini-organs that respond to diverse signals originating from multiple sources.

Results

Notch mutant mice possess fewer, but larger, sebaceous glands

Although Notch signaling is crucial for maintaining bulge stem cell identity (Demehri and Kopan, 2009), it remains unclear whether this pathway is important for stem cells in the upper follicle. In canonical Notch signaling, the transcription factor Rbpj is required to activate expression of downstream target genes. To test the role of Notch in the upper hair follicle, we therefore generated mice expressing tamoxifen-inducible *Lrig1* promoter-driven *Cre recombinase (Lrig1-Cre^{ERT2})* coupled with homozygous floxed alleles of *Rbpj* (LR mice) (Powell et al., 2012; Yamamoto et al., 2003). This enabled targeted ablation of Notch signaling in Lrig1^{+} stem cells that normally maintain the infundibulum and SGs, while preserving Notch in the bulge and secondary hair germ (Figure 1A).

Ten weeks after deleting *Rbpj* in adult resting phase (telogen) skin, we noticed by conventional histology that SGs were less abundant in LR mice; however, when persistent SGs were observed in mutants, they were enlarged (Figure 1B-C). Since SG size can vary by hair cycle stage and gender (Azzi et al., 2006; Reichenbach et al., 2018), we analyzed only telogen skin and confirmed all major findings in this study using grouped and gender-segregated analyses.

To gain a more comprehensive view, we turned to whole-mounts (WMs) of dorsal skin. Conventional WM techniques are typically performed on tail skin, since dorsal skin follicles

often fracture during dermal-epidermal separation. However, when we stabilized dorsal skin with an adhesive substrate, we found that intact follicles and SGs could be reliably recovered (Figure 1D). This modified WM technique paved the way for quantitative approaches for measuring SG size, number, shape and 3-dimensional spatial relationships, enabling us to assess SGs from >20,000 follicles for this study.

Using the modified WM approach, we confirmed that most follicles possess paired SG lobes. For control samples, we typically observed ~1.9 lobes per follicle (19 lobes per 10 follicles) (Figure 1E). It remains unclear whether the occasional absence of SG lobes is physiological or due to limitations of this technique, including instances where paired lobes may be folded over to appear as a single aggregate. Nonetheless, our WMs confirmed that LR follicles possessed fewer SG lobes (Figure 1E, S1A-C). This was especially apparent when we assessed the distribution of follicles bearing 2 SG lobes (2-SG), a single lobe (1-SG) or no lobes (0-SG) (Figure 1F). Since 1-SG follicles stably maintained a single SG lobe even after its partner had been ablated (Figures 1G, S1B), this provides functional evidence that each lobe is likely maintained by its own dedicated stem cell population.

Finally, our WM analyses confirmed that persistent SGs in LR mice were enlarged (Figure 1H, S1A). This enlargement was seen even when mutant SGs, which were often 1-SGs, were compared specifically against 1-SGs that were occasionally seen in controls (Figure S1A). Furthermore, we determined by conventional histology that mutant SGs enlarged due to increased numbers of sebocytes per gland, not due to changes in overall sebocyte size (Figures 1I-J). We also noted that higher TAM doses ablated Rbpj and SGs more thoroughly, and accelerated the enlargement of rare persistent lobes (Figures 1K-L, S1D). This suggests that 1-SGs likely arose following incomplete Cre-mediated deletion of *Rbpj* within individual SG stem cell niches. Lastly, we determined that losing a single copy of *Rbpj* did not cause SG defects in heterozygous mice (Figure S1E). Based on these findings, we were thus confronted with two seemingly related, but contradictory, phenomena: Overall loss of SG lobes in LR mice, but also gain in individual SG size. We therefore set off to reconcile these phenotypes below.

Loss of *Rbpj* in SG stem cells inhibits sebocyte differentiation

Notch deletion has previously been reported to induce epidermal differentiation at the expense of hair follicles (Demehri and Kopan, 2009; Yamamoto et al., 2003). Since LR mice lose SGs, this suggests that Notch may also be crucial for promoting sebocyte differentiation. We therefore first characterized the Notch pathway in wild-type SGs, and noted that Lrig1^{+} stem cells along the periphery of the SG expressed Rbpj and markers of Notch pathway activation (Figure 2A). These markers were especially prominent in cells at the proximal tip of the gland, a site where initial sebocyte differentiation has been proposed to occur (Kretzschmar et al., 2014). In contrast, LR mice frequently possessed “finger-like” epithelial remnants instead of SGs. These fingers lacked Rbpj and Hes1, but uniquely displayed a “speckled” pattern of minute lipid droplet accumulation up to 20 weeks post-TAM (Figures 1G, 2A).

We next assessed a panel of SG and keratin markers in wild-type SGs, and confirmed that proximal tip cells expressed early sebocyte differentiation markers such as androgen

receptor (AR) and peroxisome proliferator-activated receptor γ (PPARγ), but not late stage markers like fatty acid synthase (FASN) (Cottle et al., 2013) (Figure 2B). Furthermore, SG basal layer stem cells expressed keratins (K) 5 and 14, whereas differentiated sebocytes expressed K14 and K79, but had reduced K5 (Veniaminova et al., 2013) (Figure 2C, S2A). These findings suggest that SG lower tip cells may represent a transitional state that can be minimally defined by co-expression of a basal layer stem cell marker (K5) and an early sebocyte differentiation marker (PPARγ) (Figure S2B).

In LR finger-like remnants, we noticed that these stage-specific differentiation markers became intermingled (Figures 2B-C). LR fingers were proliferative (Figure 2D), displayed diffuse AR and PPARγ, and were $K79^{+}$ but $FASN^{-}$, features that do not normally co-occur within the SG. At early timepoints post-TAM, we also observed initial conversion of SGs into fingers starting from the bottom tip of the gland (Figure 2E). While these observations are consistent with the view that sebocyte differentiation occurs at the lower-most region of the gland, progenitor cells may also differentiate from other sites in the SG, as recently demonstrated by multi-color lineage tracing (Andersen et al., 2019).

Altogether, our findings suggest that upon differentiation, SG basal layer cells switch from a K14:K5 pairing to a K14:K79 pairing, for which we will provide additional evidence below. Rbpj promotes sebocyte formation, and in its absence, SG stem cells likely initiate early stages of differentiation, but cannot complete later stages. As a consequence, these Rbpj-deficient SG progenitors become trapped in an unnatural hybrid state where stem and differentiation features are intermixed, and lipid droplet accumulation is initiated, but stalled. Our observations do not indicate that losing Rbpj increases apoptosis in the gland (Figure S2C), or causes SG progenitors to fully convert into epidermis, as summarized in Figure 2F.

SGs do not enlarge to compensate for loss of partner lobes

If Rbpj's sole function is to promote SG differentiation, why then do a subset become enlarged in LR mice? To address this, we first determined that enlarged SGs maintained Rbpj expression, confirming that these glands had escaped Cre-mediated recombination (Figure 3A). We next hypothesized that these "escaped" SGs might somehow sense the loss of partner lobes and expand in order to compensate (Figure 3B).

To test this, we examined rare 2-SGs that persisted in LR mice and determined that these lobes were enlarged, indicating that lobe loss is not required for SG expansion (Figures 3C-D). Conversely, by administering low doses of TAM to LR mice (LR-low), we achieved extremely limited deletion of Rbpj and SGs in male mice (Figure 3E-F, S3A-B). When we specifically assessed 1-SGs from these LR-low males, singlet lobes were not enlarged (Figure 3G). This indicates that losing one SG lobe does not necessarily lead to expansion of its partner, suggesting that SG stem cells within each lobe behave independently. Female mice displayed extensive SG loss even with low TAM (Figure 3F) and could not be interpreted for these studies.

To validate that loss of SGs is due to disruption of Notch signaling, and not merely due to deletion of Rbpj, we further analyzed mice expressing *Lrig1-Cre*^{ERT2} and homozygous

Notch1 floxed alleles (LN1 mice) to ablate the Notch1 receptor (Yang et al., 2004). LN1 SGs displayed a variety of deformities, ranging from lobe loss to the appearance of miniaturized lobes that retained the ability to express differentiation markers such as FASN and accumulate lipids (Figure 3H-I, S3C-D). These observations are consistent with the view that deleting individual Notch receptors causes a partial disruption of Notch signaling, resulting in less detrimental phenotypes compared to those associated with complete suppression of the pathway via deletion of Rbpj. Altogether, these data provide functional evidence that the Notch pathway promotes SG differentiation, and that each individual SG lobe is serviced by independently-behaving stem cell populations that do not sense the presence or absence of partner lobes. Below, we provide evidence for an alternative mechanism that likely explains why persistent SGs become enlarged in mutant LR mice.

Loss of *Rbpj* in the IFE likely promotes SG expansion

During homeostasis, Lrig1$^+$ stem cells normally replenish the hair follicle infundibulum (INF), but not the interfollicular epidermis (IFE) (Page et al., 2013). Losing Notch, however, enables mutant cells in the skin to expand beyond their normal territories (Demehri and Kopan, 2009; Vagnozzi et al., 2015; Veniaminova et al., 2013), possibly explaining why LR mice exhibit increased proliferation in SG, INF and also IFE compartments (Figure 4A, S3E). We therefore quantitated Rbpj$^+$ cells in LR skin, and observed initial loss of Rbpj in the INF, but not in the IFE or bulge (Figure 4B-C, S3F-G). Over time, continuous patches of mutant Rbpj$^-$ cells extended out from the INF and replaced Rbpj$^+$ cells in the IFE (Figure 4B). This raised the possibility that in LR mice, incidental loss of Rbpj in the IFE may indirectly cause persistent SGs to expand (Figure 4D).

We tested this possibility by generating mice harboring *K14* promoter-driven *Cre^{ERT}* and homozygous *Rbpj* floxed alleles. By administering low doses of TAM to these animals (KR mice), we stably and selectively targeted *Rbpj* deletion to the IFE, while largely sparing the hair follicle (Figure 4E, S4A-C). The specificity of this approach was underscored by the emergence of clear boundaries separating mutant Rbpj$^-$ cells in the IFE, from Rbpj$^+$ cells in the adjacent hair follicle INF (Figure 4F). When we administered higher TAM doses (KR-high mice), *Rbpj* deletion was observed in follicles, although individual infundibula drifted towards becoming almost entirely Rbpj$^+$ or Rbpj$^-$ over time (Figure 4G, S4D).

Returning to KR mice, since *Rbpj* was not deleted from follicles, SGs were maintained (Figure 4H-I). Nonetheless, these SGs expanded and displayed increased proliferation, indicating that deleting *Rbpj* largely in the IFE is sufficient to recapitulate the SG enlargement phenotype seen in LR mice (Figures 4J-L, S4E-G). Consistent with these findings, KR-high mice also displayed enlarged SGs (Figure S4H). These observations suggest that Notch signaling simultaneously exerts dual opposing effects on SGs from two different stem cell niches: Whereas Notch directly promotes sebocyte differentiation from SG stem cells, this pathway also indirectly suppresses these glands from outside the SG stem compartment, likely from the IFE.

Indirect suppression of SGs by Notch is TSLP-independent

To evaluate the physiological consequences of deleting *Rbpj* in different skin compartments, we characterized the morphologies of LR and KR skin. We noted that LR mice, which lose most of their SGs, frequently developed eczematous dermatitis lesions, 10-20 weeks post-TAM (Figure S5A). In contrast, KR mice appeared largely normal and devoid of lesions up to 20 weeks post-TAM. These findings suggest that losing SGs may be critical for instigating a dermatitis-like phenotype in our system.

To delve into the molecular effects of ablating *Rbpj* in the skin, we next performed RNA-seq on LR, KR and control skin, 10 weeks post-TAM. We also performed RNA-seq on mice expressing *K14-Cre*^{ERT} and homozygous *Notch1* floxed alleles (KN1 mice), where deletion of *Notch1* was mostly targeted to the IFE, for reasons described below. By using hierarchical clustering and principal component analysis, we distinguished LR, KR and KN1 transcriptomes from litter-mate controls (Figure 5A-B). Moreover, LR and KR samples clustered more closely to one another than to KN1 samples, as expected (Figure S5B). In LR skin, 330 genes were differentially expressed (Figure 5C), and genes associated with SGs such as *K79, CIDEA* (both downregulated) and *Gata6* (upregulated) were also altered (Donati et al., 2017; Oulès et al., 2019; Swanson et al., 2019; Zhang et al., 2014). Consistent with these findings, we confirmed that Gata6^{+} cells were increased in LR follicles lacking SGs (Figure 5D, S5C).

By examining the overlap between differentially expressed genes (DEGs) in LR and KR samples versus controls, we compiled a 109 gene signature for *Rbpj* disruption in the skin ("pan-Rbpj") (Figures 5C). The degree of overlap between LR and KR gene sets was highly significant ($p = 1.08 \times 10^{-87}$), and pan-Rbpj DEGs were enriched for functional gene ontology (GO) categories such as "inflammatory response" (e.g. *CCL2, CCL22, IL23A)* and "angiogenesis" (e.g. *VEGFA, ADAM8)* (Figure 5E), processes previously reported to be increased in *Rbpj*-deficient skin (Demehri et al., 2009b; Dumortier et al., 2010). By focusing on overlapping DEGs for LR, KR and KN1 samples versus controls, we further identified 22 genes that were significantly altered across all mutant samples, regardless of whether *Rbpj* or *Notch1* had been ablated in different skin compartments ("pan-Notch") (Figures 5C). Notable genes in this category included *FLT1, DSGla, CEACAM12* and *TSLP*.

TSLP, encoding thymic stromal lymphopoietin, is a cytokine associated with a T helper 2 immune response that has previously been reported to be upregulated in atopic dermatitis and Notch-deficient skin (Demehri et al., 2009a; Demehri et al., 2012; Dumortier et al., 2010; Piazza et al., 2012). Concordantly, we confirmed upregulation of *TSLP* in LR, KR and KN1 samples (Figure 5F). To functionally test whether increased TSLP causes SG expansion, we generated LR mice in a *TSLP*- deficient background (LRT mice) (Han et al., 2012). Ten weeks post-TAM, however, we observed that loss of TSLP did not prevent SG enlargement in LRT animals (Figure 5G-I, S5D). Other genes previously shown to promote SG enlargement, including *Epgn* (Dahlhoff et al., 2014), were also upregulated upon losing *Rbpj* (up 2.1x in LR, up 3x in KR) and may well play a functional role in our system.

Loss of Notch is epistatic to gain of Hedgehog in SGs

Having uncovered multiple genes and processes that might potentially link Notch disruption in the IFE with SG expansion, we next sought to place Notch in the context of established pathways known to be crucial for SGs. We therefore turned our attention to Hedgehog (Hh) signaling, which can promote ectopic SG formation (Allen et al., 2003; Gu and Coulombe, 2008). We noted that mice expressing *Lrig1-Cre*^{ERT2} and a conditional activated allele of *Smoothened* fused to *EYFP (SmoM2)* (LS mice) (Mao et al., 2006) develop ectopic EYFP^{+} SGs, confirming that Hh directly promotes SG formation from Lrig1^{+} stem cells (Figure S6A-S6E). Hh likely also promotes SG expansion indirectly, since preexisting sebaceous lobes became enlarged, but remained EYFP^{-} (Figure S6E).

In LS mice harboring additional *Rbpj* floxed alleles (LSR mice), both preexisting and ectopic SGs disappeared and were replaced by finger-like sebaceous remnants that often retained EYFP/SmoM2 expression, indicating that loss of Notch signaling is epistatic to gain of Hh (Figure S6E). However, LSR remnants possessed noticeably larger lipid droplets compared to LR remnants (Figures S6B, S6D). This complex phenotype suggests that while loss of Notch is largely dominant to gain of Hh, Hh can still promote limited lipid accumulation even in the absence of Notch.

K79 maintains SG structural integrity

Up to this point, our studies have identified factors that can act directly or indirectly to precisely modulate SGs. Regardless of phenotype, one commonality of all SGs—whether homeostatic, ectopic or enlarged—is high expression of K79. Indeed, our characterizations above showed that when SG basal layer cells differentiate into sebocytes, this event is marked by a characteristic shift in type II keratin expression, from K5 → K79 (Figure 2C, S2A). Furthermore, gene expression network analysis incorporating gene ontology pathway enrichment analysis, using two previously published large independent datasets assaying mouse tail skin, demonstrated that expression of *K79* was significantly correlated with that of genes with the function “lipid metabolic process” ($p = 1 \times 10^{-20}$) (Quigley et al., 2016; Quigley et al., 2009) (Figure 6A). Together, these observations prompted us to examine SGs in *K79* knock-out mice, where the *K79* locus is disrupted by insertion of *LacZ* (K79-KO) (Mesler et al., 2017) (Figure 6B). Indeed, while K79-KO SGs properly accumulated oils, these glands appeared fragmented and malformed (Figures 6C, S6F).

To confirm that SG defects were not an artifact of LacZ expression in sebocytes, we also generated a conditional allele of *K79* lacking *LacZ* and coupled this with constitutive *K5* promoter-driven *Cre* (K79-cKO) (Figure 6B). K79-cKO mice recapitulated the SG defects seen in KO animals (Figures 6C, S6G). Strikingly, K79’s presumptive type I keratin binding partner, K14, was specifically de-stabilized in mutant sebocytes, but remained properly localized in surrounding SG basal layer stem cells, where K5 is expressed (Figure 6D, S2A). Although another type I keratin, K17, co-localizes with K79 in the INF and anagen follicle (Veniaminova et al., 2013), we found that K17 was hardly expressed in sebocytes and, correspondingly, SGs from K17-null dorsal skin did not possess obvious structural abnormalities (McGowan et al., 2002) (Figure 6D).

Finally, while K79-KO mice do not exhibit hair cycling defects (Mesler et al., 2017), all K79-KO and -cKO animals eventually developed dry eyes and corneal ulcers (Figure 6E). This was due to collapse of Meibomian glands in the eyelid, which normally secrete lipids to lubricate and protect the eye's surface (Figure 6E). Overall, these findings provide functional evidence that K79 maintains the structural integrity of epithelial glands, and that a K14:K5 → K14:K79 keratin shift occurs as SG basal layer stem cells differentiate into sebocytes.

Loss of *Notch1* in the IFE likely promotes SG expansion

As recent deep sequencing studies have revealed that *Notch1* is among the most frequently mutated genes in aged, sun-exposed human skin, we lastly sought to model the effects of sporadic *Notch1* mutations incurred within the adult epidermis. We therefore administered low doses of TAM to a cohort of female KN1 mice to induce highly restricted deletion of *Notch1* in the IFE. Over 32 weeks, this led to nearcomplete replacement of normal IFE with mutant $Notch1^{-}$ keratinocytes that only occasionally extended into follicles (Figure 7A). Similar to *Rbpj* deletion, clear boundaries frequently emerged at junctions between $Notch1^{-}$ IFE and $Notch1^{+}$ hair follicle epithelium (Figure 7B). Although mutant mice did not exhibit overt skin defects, their SGs were enlarged relative to gender-matched littermate controls (Figure 7C, S7A). These changes were modest but statistically significant, suggesting that losing *Notch1* in the IFE may cause chronic, low level perturbations that promote SG expansion over time. Consistent with this, RNA-seq analysis identified 330 DEGs in KN1 skin versus controls, enriched for GO categories such as "intermediate filament," "skin development" and "extracellular matrix" (Figure 5C, E).

Finally, we asked whether SG enlargement during aging is associated with loss of Notch pathway components in the IFE. Although we confirmed that SGs were indeed expanded in 75-week old wild-type animals compared to young mice in a C57BL/6 background (Figure 7D, S7B), as previously reported (Han et al., 2006), neither loss of Notch1 nor Rbpj was detected in the skin (Figure 7A, S7C). Loss of either gene might not be expected, since laboratory mice are not exposed to sunlight and, consequently, UV-induced DNA damage. Altogether, these findings suggest that SGs can enlarge during physiological aging without losing Notch pathway components. At the same time, genetic perturbations that are highly relevant to aged, sun-exposed human skin, including mutations in Notch receptors, may act on top of physiological aging to further promote SG expansion.

Discussion

SGs are complex mini-organs whose size and activity are intricately regulated. When we first observed that LR mice possess fewer, but larger, SGs, this initially suggested to us a compensatory response, reminiscent of previous findings in hair follicles, where ablation of specific stem cell populations forces neighboring cells to compensate (Rompolas et al., 2013). Such a response might conceivably occur if SGs are able to sense a reduction in sebum, either locally in the hair canal or throughout the skin's surface, and enlarge in order to increase lipid production.

Although we cannot rule out this possibility, our data do not suggest that compensation drives SG expansion in our system. Indeed, we observed that SGs can expand without losing

lobes, whereas conversely lobe loss does not always cause SG enlargement. Furthermore, the appearance of unpaired, singlet 1-SGs in LR follicles strongly argues against the existence of a common stem cell pool that maintains both lobes in the hair follicle. Instead, our data provide functional evidence suggesting that each individual SG lobe is likely serviced by its own dedicated, independently-behaving stem cell population. While these populations do not appear to influence one another, they are acutely responsive to genetic perturbations in the epidermis.

In aged sun-exposed human skin, these genetic perturbations often occur in genes encoding Notch receptors (Lynch et al., 2017; Martincorena et al., 2015). This is likely due to the relentless expansion of Notch-deficient cell clones that exhibit impaired differentiation (Lowell et al., 2000; Vagnozzi et al., 2015). Despite the ubiquity of these mutations, however, it remains unclear how sporadic Notch mutations sustained during adulthood affect the skin as we age. Previous studies in mice have typically relied upon constitutive deletion of Notch components, induced either during development or within days after birth (Blanpain et al., 2006; Demehri et al., 2009a; Dumortier et al., 2010; Pan et al., 2004; Vauclair et al., 2005; Yamamoto et al., 2003). This leads to profound phenotypes, including hyperkeratosis, hair follicle destruction, cyst formation and severe inflammation. Owing to these general defects, the question of how Notch modulates SG stem cells has been difficult to address. Furthermore, in studies where Notch components were conditionally deleted in adult mice, SG defects were not noted (Demehri and Kopan, 2009; Murthy et al., 2012; Weber et al., 2011).

By performing targeted, low level ablation of Notch in specific stem cell niches, balanced with gradual expansion of mutant cell clones, our studies help unravel the direct and indirect effects of this pathway on SGs in adult skin. Our observations highlight the complexity by which cells in different compartments within the same organ interact to maintain proper tissue function. Ultimately, cell fate decisions are made based on the integration of multiple —and, at times, contradictory—signals originating both locally and afar (Hsu and Fuchs, 2012). With this level of interconnectedness, it is perhaps not surprising that defects in Notch manifest SG phenotypes that are more complex and subtle than a traditional “1 gene = 1 phenotype” model.

Given prior reports of severe skin defects in Notch-deficient mice, what was unexpected was the mild phenotype of KR mice, where *Rbpj* was deleted specifically in the adult IFE (Figure S5A). Indeed, these animals did not possess overt skin defects even though loss of Rbpj was sustained long-term. While we cannot rule out the possibility that SG expansion in KR mice mitigated the effects of losing Rbpj in the IFE, this is nonetheless in stark contrast to LR mice, which developed dermatitis, akin to previous studies (Demehri et al., 2009a; Dumortier et al., 2010). These findings suggest that SG disruption may be a critical driver for skin disease. Indeed, an immune-modulatory role for sebum has been hypothesized to control eczematous dermatitis, a frequent side-effect of anti-acne medications that suppress sebum production (Lovászi et al., 2017; Shi et al., 2015). In addition, sebum secretion rates vary throughout life and are inversely correlated with the incidence of atopic dermatitis (Shi et al., 2015; Zouboulis and Boschnakow, 2001). In humans, certain lipid species such as squalene and wax esters are found only in sebum (Smith and Thiboutot, 2008). Thus, it will

be critical in future studies to evaluate the relative importance of epidermal- versus SG-derived lipids in modulating eczematous disorders.

During physiological aging, lipid content also decreases in the skin (Rittié and Fisher, 2015). Although facial SGs become enlarged, sebum production is reduced, possibly explaining why aged skin is more prone to becoming xerotic and pruritic. It remains unclear why SG size and secretory output change over time, but these effects may be related to shifts in hormones such as androgen, alterations in IGF signaling, accumulation of oxidative stress, senescence, and changes in the dermis, ultimately leading to reduced sebocyte turnover (Zouboulis and Boschnakow, 2001). Superimposed upon chronological aging, our data suggest that *Notch1* mutations sustained in the IFE may also indirectly promote SG enlargement over time, which may be especially relevant to photoaged skin that displays both SG hyperplasia and high mutational burden.

Altogether, by analyzing a diverse array of SG phenotypes (Figure 7E), our studies help untangle some of the complex signals that act simultaneously to regulate these glands. We find that Notch signaling directly promotes differentiation in SG stem cells, and also indirectly suppresses these glands from outside their stem cell compartment. Loss of Notch is epistatic to gain of Hh signaling, which can both directly and indirectly promote SG formation and enlargement. Finally, while keratins in human SGs have been described (Zouboulis et al., 1994), the identity of SG keratins in mice has been enigmatic. Using bioinformatic and functional studies, we now show that sebocyte differentiation is associated with a K14:K5→K14:K79 switch, and that K79 is crucial for maintaining the integrity of SGs and Meibomian glands. In light of these findings, additional studies will be needed to determine whether gain of K79 induces SG hyperplasia, and whether loss of K79 may be an underlying cause of syndromes such as chronic dry eye disease.

STAR METHODS

CONTACT FOR REAGENT AND RESOURCE SHARING

Further information and requests for resources and reagents should be directed to and will be fulfilled by the Lead Contact, Sunny Wong (sunnyw@umich.edu).

Rpb-j^{flox} and *TSLP-KO* mice were obtained under an MTA and can be distributed only after formal approval is granted from their institute of origin.

EXPERIMENTAL MODEL AND SUBJECT DETAILS

Animal Models—All mice were induced with tamoxifen at 8 weeks of age, using the following doses: For LR, LN1, LS and LSR strains: 1 mg/40 grams body weight (1 dose). For LR-high mice: 1 mg/40 grams body weight (3 daily doses). For LR-low mice: 0.3 mg/40 grams body weight (1 dose). For KR mice: 0.8 mg/40 grams body weight (1 dose). For KR-high mice: 1 mg/40 grams body weight (2 doses). For KN1 mice: 0.5 mg/40 grams body weight (1 dose). For information regarding animal strains, please refer to the Key Resources Table. Except for KN1 studies which utilized only female mice, all other studies were performed on mice of both genders in a mixed genetic background, using littermate animals for comparisons when possible. All mice were maintained in specific pathogen free housing

and were used in accordance with regulations established by the University of Michigan Unit for Laboratory Animal Medicine.

METHOD DETAILS

Tamoxifen—Tamoxifen was dissolved in corn oil by vortexing for 2 hours at room temperature. A volume of 200 μL tamoxifen solution was injected intraperitoneally per 20 grams mouse body weight.

Whole Mounts—For whole-mount analysis, telogen dorsal skin (~1 cm^2) was collected, stretched on a paper towel, and covered with Elmer's No-Wrinkle Rubber Cement. Five minutes later, clear tape was affixed to the surface of the skin. The sample was pressed flat, trimmed, and floated on freshly prepared 5 mM EDTA/PBS for 6 hours at 37 degrees Celsius. Afterwards, the taped epidermis was separated from the dermis using fine forceps and fixed in neutral buffered formalin for 30 minutes at room temperature. Samples were then washed, and stained with Nile Red (4 μg/ml) and DAPI (1 μg/ml) for 30 minutes in PBS with gentle shaking at room temperature in the dark. Finally, samples were mounted with Vectashield on microscope slides, and images were taken within 24 hours.

Immunohistochemistry—Frozen sections were probed using antibodies against the following antigens and at the following dilutions: AR (1:150), Gata6 (1:300), GFP (1:500), Ki67 (1:300), K5 (1:500), K14 (1:500, Covance), K17 (1:1000), K79 (1:400, Santa Cruz), K79 (1:1000, Abcam), Lrig1 (1:800), PPARγ (1:200), and TSLP (1:300). Frozen sections were probed using antibodies against the following antigens, and subsequently amplified by TSA Fluorescein Plus kit: Hes1 (1:500), NICD (1:500), Notch1 (1:300), and Rbpj (1:300). Paraffin-embedded sections were antigen-retrieved by simmering slides in 1 mM EDTA, pH 8.0, for 20 minutes, and probed using antibodies against the following antigens: cleaved caspase-3 (1:300) and Rbpj (1:300). Both frozen and paraffin-embedded sections were stained using antibodies against the following antigens: FASN (1:200) and K14 (1:500, Santa Cruz). In some cases, fluorescence images were processed using the Auto-Blend feature of Adobe Photoshop CS6 to automatically maximize image sharpness across multiple focal planes.

RNA Collection—Telogen dorsal skin was shaved and a ~4 × 4 cm region of skin was collected and incubated overnight in 0.25% trypsin at 4 degrees Celsius. The next day, the epidermis were scraped from the dermis using a razor blade, minced in trypsin, and passed through a 100 μm nylon mesh to remove hair shafts. The cells were lysed in 350 μL RLT buffer per 5 × 10^6 cells, and processed using RNeasy Mini Kit. 1.5 μg of total RNA with RIN ≥ 7 was submitted to Novogene Corporation for RNA-Seq, and ~20 × 10^6 reads were collected per sample.

RNA-Seq Analysis—Samples analyzed by RNA-Seq included 3 LR mice and 3 matched controls (batch 1); 4 KR mice and 2 matched controls (batch 2); and 4 KN1 mice and 2 matched controls (batch 3). All samples were harvested from telogen dorsal skin, 10 weeks post-TAM. RNA-seq was performed using 150 bp pairedend reads. Reads were aligned with STAR using the mm10 reference genome. Gene quantitation was conducted by HTSeq,

using the GENCODE v18 gene model. Analyses were performed using DESeq2, and DEGs were determined by using a negative binomial model comparing mutant and matched control samples within each batch, using a False Discovery Rate (FDR) threshold of 10% and $|\log_2$ fold-change$| \geq 1$. Functional enrichment analyses were performed using DAVID.

K79 Network Analysis—*K79* expression was compared to that of other genes in two independent previously published collections of tail skin gene expression (N = 248, N = 71) (Quigley et al., 2016; Quigley et al., 2009). Microarray results were processed as previously described. Non-parametric Spearman correlation values were calculated in R. FDR values were calculated from unadjusted correlation *P* values using the "BH" method of R's*p.adjust* function. 350 genes were significantly correlated with *K79* expression in both datasets at a FDR threshold of 1%. Of these 350 genes, 74 had a correlation value of ≥ 0.40 across both datasets and were enriched for harboring the annotation "lipid metabolic process" (N = 25, $p = 1 \times 10^{-20}$). Gene Ontology analysis was performed using BiNGO (Maere et al., 2005), and the gene network was displayed using Cytoscape (Shannon et al., 2003). Similar results were obtained using DAVID (Huang et al., 2009), where "lipid metabolic process" was enriched ($p = 3.9 \times 10^{-17}$).

QUANTIFICATION AND STATISTICAL ANALYSIS

SG Quantitation—For conventional H&E quantitation, at least 2 males and 2 females per genotype, per timepoint, were analyzed. To assess SG size, 5 adjacent H&E fields per specimen were taken at 20X magnification, and SG size was measured using AxioVision 4 software. The presence or absence of SGs was also noted for each follicle.

To assess SG size and number in whole-mounts, a minimum of 4 males and 4 females per genotype, per timepoint, were analyzed for most analyses. Each experiment utilized matched control animals that were either litter-mates or shared the same parents, whenever possible. Two representative fields at 5x magnification were photographed for DAPI and Nile Red staining, and subsequently all images were divided into thirds by drawing guide lines. SG size and lobe number were assessed for every 3rd complete hair follicle that intersected these guide lines, yielding ~18-25 randomly selected follicles per image. SG size was measured in pixel units using AxioVision 4 software. In most instances, individual SG lobes were located to either side of the HF, and these were outlined for size measurements. In some cases, SG aggregates located near the center of the telogen follicle displayed an "inverted 'V' (/\)" configuration; these were considered 2-SGs, with a line drawn vertically through the central indentation to divide the gland into separate lobes to quantitate size. If a SG aggregate was not observed to possess a clear indentation, this was regarded as a single lobe. Finger-like epithelial remnants in mutant mice were scored as negative for SG.

Quantifying Notch$^+$ cells and proliferation—For quantitation of Notch1$^+$/Rbpj$^+$ cells and proliferation, a minimum of 2 males and 2 females per genotype, per timepoint, were analyzed. Paraffin samples were immunostained for Rbpj, and the percentage of Rbpj$^+$ cells was quantitated along the basal layer of the IFE, and in the entire INF or bulge. Similar methods were used to quantitate Notch1$^+$ and Ki67$^+$ cells, using frozen sections.

Statistics—All SG quantitation data are depicted as means from independent biological replicates, and unpaired ttests were performed to determine statistical significance. Error bars are depicted as SEM and p-values are shown in the figure legends.

DATA AND CODE AVAILABILITY

RNA-seq data generated for this study are available through the GEO repository (GSE125737).

Supplementary Material

Refer to Web version on PubMed Central for supplementary material.

Acknowledgements

We are grateful to our colleagues at the University of Michigan (Drs. P. Coulombe, L. Samuelson, X. Fan, N. Lukacs, T. Saunders) and at the Benaroya Research Institute (Dr. S. Ziegler) for sharing mice. S.Y.W. acknowledges the support of the NIH (R01AR065409); the American Cancer Society; the Leo Foundation; the Biological Sciences Scholars Program; and the Center for Organogenesis. L.C.T. is supported by the NIH (AR072129); the Arthritis National Research Foundation; and the National Psoriasis Foundation. D.A.Q acknowledges a Prostate Cancer Foundation Young Investigator award. A.B. acknowledges support from the NCI (UO1CA176287 and R35CA210018). A.A.D. acknowledges support from the NIH (AR045973).

REFERENCES

Allen M, Grachtchouk M, Sheng H, Grachtchouk V, Wang A, Wei L, Liu J, Ramirez A, Metzger D, Chambon P, et al. (2003). Hedgehog signaling regulates sebaceous gland development. Am J Pathol 163, 2173–2178. [PubMed: 14633591]

Anders S, Pyl PT, and Huber W (2015). HTSeq--a Python framework to work with high-throughput sequencing data. Bioinformatics 31, 166–169. [PubMed: 25260700]

Andersen MS, Hannezo E, Ulyanchenko S, Estrach S, Antoku Y, Pisano S, Boonekamp KE, Sendrup S, Maimets M, Pederson MT, et al. (2019). Tracing the cellular dynamics of sebaceous gland development in normal and perturbed states. Nat Cell Biol, 10.1038/s41556-41019-40362-x.

Azzi L, El-Alfy M, and Labrie F (2006). Gender differences and effects of sex steroids and dehydroepiandrosterone on androgen and oestrogen alpha receptors in mouse sebaceous glands. Br J Dermatol 154, 21–27. [PubMed: 16403089]

Blanpain C, Lowry WE, Pasolli HA, and Fuchs E (2006). Canonical notch signaling functions as a commitment switch in the epidermal lineage. Genes Dev 20, 3022–3035. [PubMed: 17079689]

Candi E, Schmidt R, and Melino G (2005). The cornified envelope: a model of cell death in the skin. Nat Rev Mol Cell Biol 6, 328–340. [PubMed: 15803139]

Cottle DL, Kretzschmar K, Schweiger PJ, Quist SR, Gollnick HP, Natsuga K, Aoyagi S, and Watt FM (2013). c-MYC-induced sebaceous gland differentiation is controlled by an androgen receptor/p53 axis. Cell Rep 3, 427–441. [PubMed: 23403291]

Dahlhoff M, Camera E, Schäfer M, Emrich D, Riethmacher D, Foster A, Paus R, and Schneider MR (2016). Sebaceous lipids are essential for water repulsion, protection against UVB-induced apoptosis, and ocular integrity in mice. Development 143, 1823–1831. [PubMed: 26989175]

Dahlhoff M, Frances D, Kloepper JE, Paus R, Schafer M, Niemann C, and Schneider MR (2014). Overexpression of Epigen during embryonic development induces reversible, epidermal growth factor receptor-dependent sebaceous gland hyperplasia. Mol Cell Biol 34, 3086–3095. [PubMed: 24891618]

Demehri S, and Kopan R (2009). Notch signaling in bulge stem cells is not required for selection of hair follicle fate. Development 136, 891–896. [PubMed: 19211676]

Demehri S, Morimoto M, Holtzman MJ, and Kopan R (2009a). Skin-derived TSLP triggers progression from epidermal-barrier defects to asthma. PLoS Biol 7, e1000067. [PubMed: 19557146]

Demehri S, Turkoz A, and Kopan R (2009b). Epidermal Notch1 loss promotes skin tumorigenesis by impacting the stromal microenvironment. Cancer Cell 16, 55–66. [PubMed: 19573812]

Demehri S, Turkoz A, Manivasagam S, Yockey LJ, Turkoz M, and Kopan R (2012). Elevated epidermal thymic stromal lymphopoietin levels establish an antitumor environment in the skin. Cancer Cell 22, 494–505. [PubMed: 23079659]

Donati G, Rognoni E, Hiratsuka T, Liakath-Ali K, Hoste E, Kar G, Kayikci M, Russell R, Kretzschmar K, Mulder KW, et al. (2017). Wounding induces dedifferentiation of epidermal Gata6+ cells and acquisition of stem cell properties. Nat Cell Biol 19, 603–613. [PubMed: 28504705]

Doupe DP, and Jones PH (2012). Interfollicular epidermal homeostasis: dicing with differentiation. Exp Dermatol 21, 249–253. [PubMed: 22417300]

Dumortier A, Durham AD, Piazza MD, Vauclair S, Koch U, Ferrand G, Ferrero I, Demehri S, Song LL, Farr AG, et al. (2010). Atopic dermatitis-like disease and associated lethal myeloproliferative disorder arise from loss of Notch signaling in the murine skin. PLoS One 5, e9258. [PubMed: 20174635]

Ehrmann C, and Schneider MR (2016). Genetically modified laboratory mice with sebaceous glands abnormalities. Cell Mol Life Sci.

Füllgrabe A, Joost S, Are A, Jacob T, Sivan U, Haegebarth A, Linnarsson S, Simons BD, Clevers H, Toftgård R, et al. (2015). Dynamics of Lgr6+ progenitor cells in the hair follicle, sebaceous gland, and interfollicular epidermis. Stem Cell Reports 5, 843–855. [PubMed: 26607954]

Ghazizadeh S, and Taichman LB (2001). Multiple classes of stem cells in cutaneous epithelium: a lineage analysis of adult mouse skin. EMBO J 20, 1215–1222. [PubMed: 11250888]

Gu LH, and Coulombe PA (2008). Hedgehog signaling, Keratin 6 induction, and sebaceous gland morphogenesis. Am J Pathol 173, 752–761. [PubMed: 18688029]

Han G, Li AG, Liang YY, Owens P, He W, Lu S, Yoshimatsu Y, Wang D, Dijke PT, Lin X, et al. (2006). Smad7-induced beta-catenin degradation alters epidermal appendage development. Dev Cell 11, 301–312. [PubMed: 16950122]

Han H, Xu W, Headley MB, Jessup HK, Lee KS, Omori M, Comeau MR, Marshak-Rothstein A, and Ziegler SF (2012). Thymic stromal lymphopoietin (TSLP)-mediated dermal inflammation aggravates experimental asthma. Mucosal Immunol 5, 342–351. [PubMed: 22354320]

Hardman MJ, Sisi P, Banbury DN, and Byrne C (1998). Patterned acquisition of skin barrier function during development. Development 125, 1541–1552. [PubMed: 9502735]

Hsu YC, and Fuchs E (2012). A family business: stem cell progeny join the niche to regulate homeostasis. Nat Rev Mol Cell Biol 13, 103–114. [PubMed: 22266760]

Huang Da W, Sherman BT, and Lempicki RA (2009). Systematic and integrative analysis of large gene lists using DAVID bioinformatics resources. Nat Protoc 4, 44–57. [PubMed: 19131956]

Jensen KB, Collins CA, Nascimento E, Tan DW, Frye M, Itami S, and Watt FM (2009). Lrig1 expression defines a distinct multipotent stem cell population in mammalian epidermis. Cell Stem Cell 4, 427–439. [PubMed: 19427292]

Karnik P, Tekeste Z, McCormick TS, Gilliam AC, Price VH, Cooper KD, and Mirmirani P (2009). Hair follicle stem cell-specific PPARgamma deletion causes scarring alopecia. J Invest Dermatol 129, 1243–1257. [PubMed: 19052558]

Kobayashi T, Voisin B, Kim DY, Kennedy EA, Jo JH, Shih HY, Truong A, Doebel T, Sakamoto K, Cui CY, et al. (2019). Homeostatic control of sebaceous glands by innate lymphoid cells regulates commensal bacteria equilibrium. Cell 176, 982–997. [PubMed: 30712873]

Kretzschmar K, Cottle DL, Donati G, Chiang MF, Quist SR, Gollnick HP, Natsuga K, Lin KI, and Watt FM (2014). BLIMP1 is required for postnatal epidermal homeostasis but does not define a sebaceous gland progenitor under steady-state conditions. Stem Cell Reports 3, 620–633. [PubMed: 25358790]

Lovászi M, Szegedi A, Zouboulis CC, and Törőcsik D (2017). Sebaceous-immunobiology is orchestrated by sebum lipids. Dermatoendocrinol 9, e1375636. [PubMed: 29484100]

Lowell S, Jones P, Roux IL, Dunne J, and Watt FM (2000). Stimulation of human epidermal differentiation by delta-notch signalling at the boundaries of stem-cell clusters. Curr Biol 10, 491–500. [PubMed: 10801437]

Lynch MD, Lynch CNS, Craythorne E, Liakath-Ali K, Mallipeddi R, Barker JN, and Watt FM (2017). Spatial constraints govern competition of mutant clones in human epidermis. Nat Commun 8, 1119. [PubMed: 29066762]

Maere S, Heymans K, and Kuiper M (2005). BiNGO: a Cytoscape plugin to assess overrepresentation of gene ontology categories in biological networks. Bioinformatics 21, 3448–3449. [PubMed: 15972284]

Mao J, Ligon KL, Rakhlin EY, Thayer SP, Bronson RT, Rowitch D, and McMahon AP (2006). A novel somatic mouse model to survey tumorigenic potential applied to the Hedgehog pathway. Cancer Res 66, 10171–10178. [PubMed: 17047082]

Martincorena I, Roshan A, Gerstung M, Ellis P, Loo PV, McLaren S, Wedge DC, Fullam A, Alexandrov LB, Tubio JM, et al. (2015). Tumor evolution. High burden and pervasive positive selection of somatic mutations in normal human skin. Science 348, 880–886. [PubMed: 25999502]

Matsumura H, Mohri Y, Binh NT, Morinaga H, Fukuda M, Ito M, Kurata S, Hoeijmakers J, and Nishimura EK (2016). Hair follicle aging is driven by transepidermal elimination of stem cells via COL17A1 proteolysis. Science 351, aad4395. [PubMed: 26912707]

McGowan KM, Tong X, Colucci-Guyon E, Langa F, Babinet C, and Coulombe PA (2002). Keratin 17 null mice exhibit age- and strain-dependent alopecia. Genes Dev 16, 1412–1422. [PubMed: 12050118]

Mesler AL, Veniaminova NA, Lull MV, and Wong SY (2017). Hair follicle terminal differentiation is orchestrated by distinct early and late matrix progenitors. Cell Rep 19, 809–821. [PubMed: 28445731]

Murthy A, Shao YW, Narala SR, Molyneux SD, Zúñiga-Pflücker JC, and Khokha R (2012). Notch activation by the metalloproteinase ADAM17 regulates myeloproliferation and atopic barrier immunity by suppressing epithelial cytokine synthesis. Immunity 36, 105–119. [PubMed: 22284418]

Niemann C, and Horsley V (2012). Development and homeostasis of the sebaceous gland. Semin Cell Dev Biol 23, 928–936. [PubMed: 22960253]

Nowell C, and Radtke F (2013). Cutaneous Notch signaling in health and disease. Cold Spring Harb Perspect Med 3, a017772. [PubMed: 24296353]

Oulès B, Rognoni E, Hoste E, Gross G, Fiehler R, Natsuga K, Quist S, Mentink R, Donati G, and Watt FM (2019). Mutant Lef1 controls Gata6 in sebaceous gland development and cancer. EMBO J 38, e100526. [PubMed: 30886049]

Page ME, Lombard P, Ng F, Gottgens B, and Jensen KB (2013). The epidermis comprises autonomous compartments maintained by distinct stem cell populations. Cell Stem Cell 13, 1–12. [PubMed: 23827700]

Pan Y, Lin MH, Tian X, Cheng HT, Gridley T, Shen J, and Kopan R (2004). Gammasecretase functions through Notch signaling to maintain skin appendages but is not required for their patterning or initial morphogenesis. Dev Cell 7, 731–743. [PubMed: 15525534]

Piazza MD, Nowell CS, Koch U, Durham AD, and Radtke F (2012). Loss of cutaneous TSLP-dependent immune responses skews the balance of inflammation from tumor protective to tumor promoting. Cancer Cell 22, 479–493. [PubMed: 23079658]

Powell AE, Wang Y, Li Y, Poulin EJ, Means AL, Washington MK, Higginbotham JN, Juchheim A, Prasad N, Levy SE, et al. (2012). The pan-ErbB negative regulator Lrig1 is an intestinal stem cell marker that functions as a tumor suppressor. Cell 149, 146–158. [PubMed: 22464327]

Quigley DA, Kandyba E, Huang P, Halliwill KD, Sjölund J, Pelorosso F, Wong CE, Hirst GL, Wu D, Delrosario R, et al. (2016). Gene expression architecture of mouse dorsal and tail skin reveals functional differences in inflammation and cancer. Cell Rep 16, 1153–1165. [PubMed: 27425619]

Quigley DA, To MD, Perez-Losada J, Pelorosso FG, Mao JH, Nagase H, Ginzinger DG, and Balmain A (2009). Genetic architecture of mouse skin inflammation and tumour susceptibility. Nature 458, 505–508. [PubMed: 19136944]

Ramirez A, Page A, Gandarillas A, Zanet J, Pibre S, Vidal M, Tusell L, Genesca A, Whitaker DA, Melton DW, et al. (2004). A keratin K5Cre transgenic line appropriate for tissue-specific or generalized Cre-mediated recombination. Genesis 39, 52–57. [PubMed: 15124227]

Rangarajan A, Talora C, Okuyama R, Nicolas M, Mammucari C, Oh H, Aster JC, Krishna S, Metzger D, Chambon P, et al. (2001). Notch signaling is a direct determinant of keratinocyte growth arrest and entry into differentiation. EMBO J 20, 3427–3436. [PubMed: 11432830]

Reichenbach B, Classon J, Aida T, Tanaka K, Genander M, and Göritz C (2018). Glutamate transporter Slc1a3 mediates inter-niche stem cell activation during skin growth. EMBO J 37, e98280. [PubMed: 29615452]

Rittié L, and Fisher GJ (2015). Natural and sun-induced aging of human skin. Cold Spring Harb Perspect Med 5, a015370. [PubMed: 25561721]

Rittié L, Tejasvi T, Harms PW, Xing X, Nair RP, Gudjonsson JE, Swindell WR, and Elder JT (2016). Sebaceous gland atrophy in psoriasis: an explanation for psoriatic alopecia? J Invest Dermatol 136, 1792–1800. [PubMed: 27312025]

Rompolas P, Mesa KR, and Greco V (2013). Spatial organization within a niche as a determinant of stem-cell fate. Nature 502, 513–518. [PubMed: 24097351]

Schepeler T, Page ME, and Jensen KB (2014). Heterogeneity and plasticity of epidermal stem cells. Development 141, 2559–2567. [PubMed: 24961797]

Schneider MR, and Paus R (2010). Sebocytes, multifaceted epithelial cells: lipid production and holocrine secretion. Int J Biochem Cell Biol 42, 181–185. [PubMed: 19944183]

Shannon P, Markiel A, Ozier O, Baliga NS, Wang JT, Ramage D, Amin N, Schwikowski B, and Ideker T (2003). Cytoscape: a software environment for integrated models of biomolecular interaction networks. Genome Res 13, 2498–2504. [PubMed: 14597658]

Shi VY, Leo M, Hassoun L, Chahal DS, Maibach HI, and Sivamani RK (2015). Role of sebaceous glands in inflammatory dermatoses. J Am Acad Dermatol 73, 856–863. [PubMed: 26386632]

Smith KR, and Thiboutot DM (2008). Thematic review series: skin lipids. Sebaceous gland lipids: friend or foe? J Lipid Res 49, 271–281. [PubMed: 17975220]

Stenn KS, Zheng Y, and Parimoo S (2008). Phylogeny of the hair follicle: the sebogenic hypothesis. J Invest Dermatol 128, 1576–1578. [PubMed: 18079744]

Swanson JB, Vagnozzi AN, Veniaminova NA, and Wong SY (2019). Loss of Gata6 causes dilation of the hair follicle canal and sebaceous duct. Exp Dermatol 28, 345–349. [PubMed: 30033638]

Vagnozzi AN, Reiter JF, and Wong SY (2015). Hair follicle and interfollicular epidermal stem cells make varying contributions to wound regeneration. Cell Cycle 14, 3408–3417. [PubMed: 26398918]

Vasioukhin V, Degenstein L, Wise B, and Fuchs E (1999). The magical touch: genome targeting in epidermal stem cells induced by tamoxifen application to mouse skin. Proc Natl Acad Sci USA 96, 8551–8556. [PubMed: 10411913]

Vauclair S, Nicolas M, Barrandon Y, and Radtke F (2005). Notch1 is essential for postnatal hair follicle development and homeostasis. Dev Biol 284, 184–193. [PubMed: 15978571]

Veniaminova NA, Vagnozzi AN, Kopinke D, Do TT, Murtaugh LC, Maillard I, Dlugosz AA, Reiter JF, and Wong SY (2013). Keratin 79 identifies a novel population of migratory epithelial cells that initiates hair canal morphogenesis and regeneration. Development 140, 4870–4880. [PubMed: 24198274]

Watt FM, Estrach S, and Ambler CA (2008). Epidermal Notch signalling: differentiation, cancer and adhesion. Curr Opin Cell Biol 20, 171–179. [PubMed: 18342499]

Weber S, Niessen MT, Prox J, Lullmann-Rauch R, Schmitz A, Schwanbeck R, Blobel CP, Jorissen E, de Strooper B, Niessen CM, et al. (2011). The disintegrin/metalloproteinase Adam10 is essential for epidermal integrity and Notch-mediated signaling. Development 138, 495–505. [PubMed: 21205794]

Yamamoto N, Tanigaki K, Han H, Hiai H, and Honjo T (2003). Notch/RBP-J signaling regulates epidermis/hair fate determination of hair follicular stem cells. Curr Biol 13, 333–338. [PubMed: 12593800]

Yang X, Klein R, Tian X, Cheng HT, Kopan R, and Shen J (2004). Notch activation induces apoptosis in neural progenitor cells through a p53-dependent pathway. Dev Biol 269, 81–94. [PubMed: 15081359]

Zhang S, Shui G, Wang G, Wang C, Sun S, Zouboulis CC, Xiao R, Ye J, Li W, and Li P (2014). Cidea control of lipid storage and secretion in mouse and human sebaceous glands. Mol Cell Biol 34, 1827–1838. [PubMed: 24636991]

Zouboulis CC, and Boschnakow A (2001). Chronological ageing and photoageing of the human sebaceous gland. Clin Exp Dermatol 26, 600–607. [PubMed: 11696064]

Zouboulis CC, Krieter A, Gollnick H, Mischke D, and Orfanos CE (1994). Progressive differentiation of human sebocytes in vitro is characterized by increasing cell size and altering antigen expression and is regulated by culture duration and retinoids. Exp Dermatol 3, 151–160. [PubMed: 8000703]

Zouboulis CC, Picardo M, Ju Q, Kurokawa I, Törőcsik D, Bíró T, and Schneider MR (2016). Beyond acne: Current aspects of sebaceous gland biology and function. Rev Endocr Metab Disord 17, 319–334. [PubMed: 27726049]

HIGHLIGHTS

- Each sebaceous gland lobe is independently maintained by a dedicated stem cell pool.
- Notch directly promotes sebaceous gland stem cell differentiation into sebocytes.
- Notch also indirectly suppresses sebaceous gland differentiation from a distance.
- Keratin 79 is crucial for maintaining sebaceous and meibomian gland structural integrity.

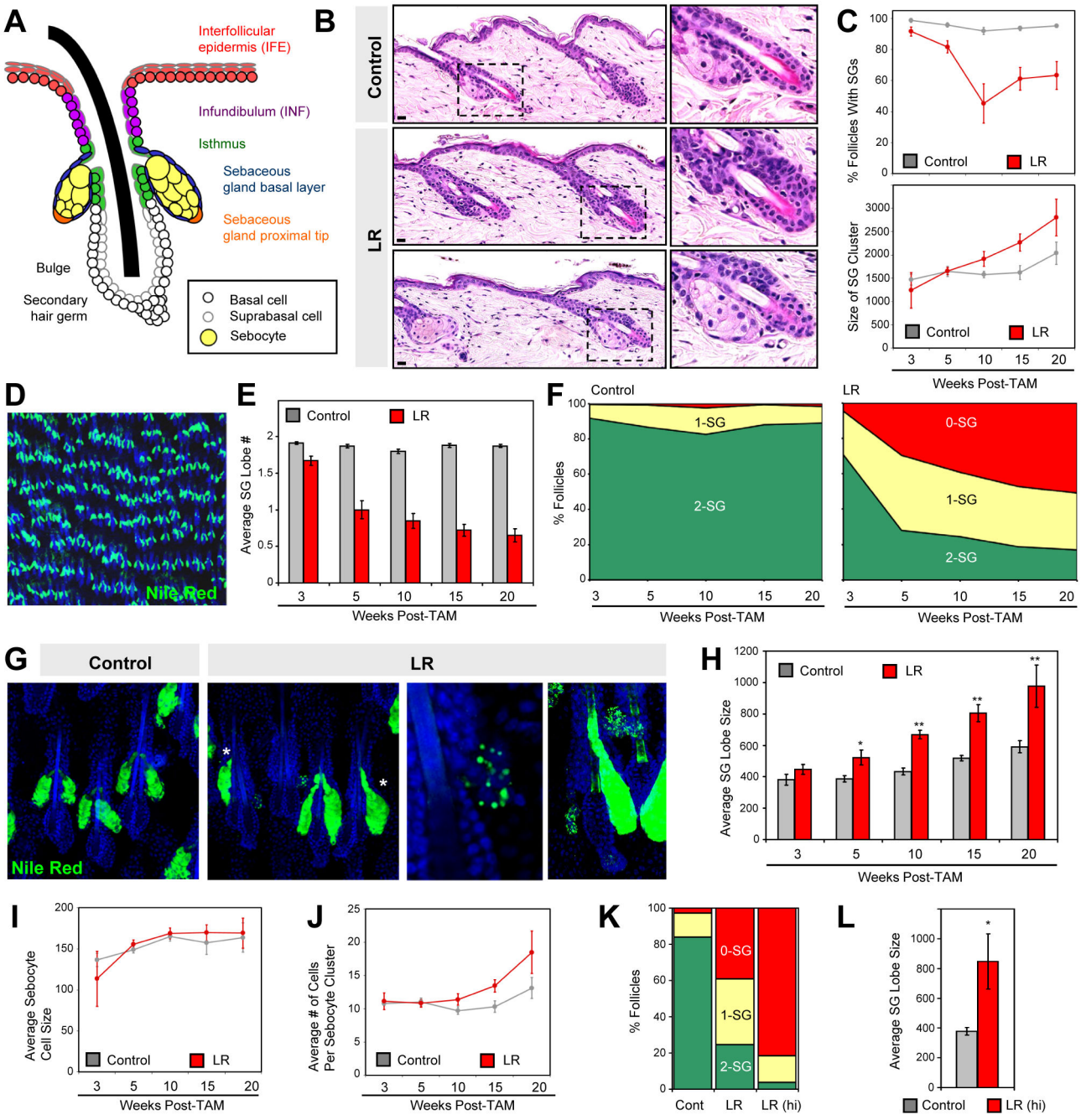

Figure 1. LR mice possess fewer, but larger, SGs.

A. Schematic of hair follicle. **B.** Skin histology, 20 weeks post-TAM. **C.** Quantitation of SG abundance and size by H&E. **D.** Example of wild-type dorsal skin with SGs stained with Nile Red (green), prepared using a modified WM technique. **E.** Quantitation of SG lobe number, per follicle, by WM. **F.** Distribution of follicles with the indicated number of SG lobes. **G.** WMs showing LR remnant fingers displaying nascent lipid droplets (arrow). Asterisks, 1-SG follicles. Right-most photo was captured with extended imaging exposure time. **H.** Quantitation of SG size by WM. **I, J.** Quantitation of sebocyte size and number by

histology. **K.** Distribution of follicles with the indicated SG lobe number by WM, 10 weeks post-TAM. Data for LR mice were from F. **L.** SG size. WM SG size measurements were made in pixel units. H&E quantitations were made in μm^2. Data are represented as mean ± SEM. *, $p < 0.05$; **, $p < 0.01$. Scale bar, 50 μm. See also Figure S1.

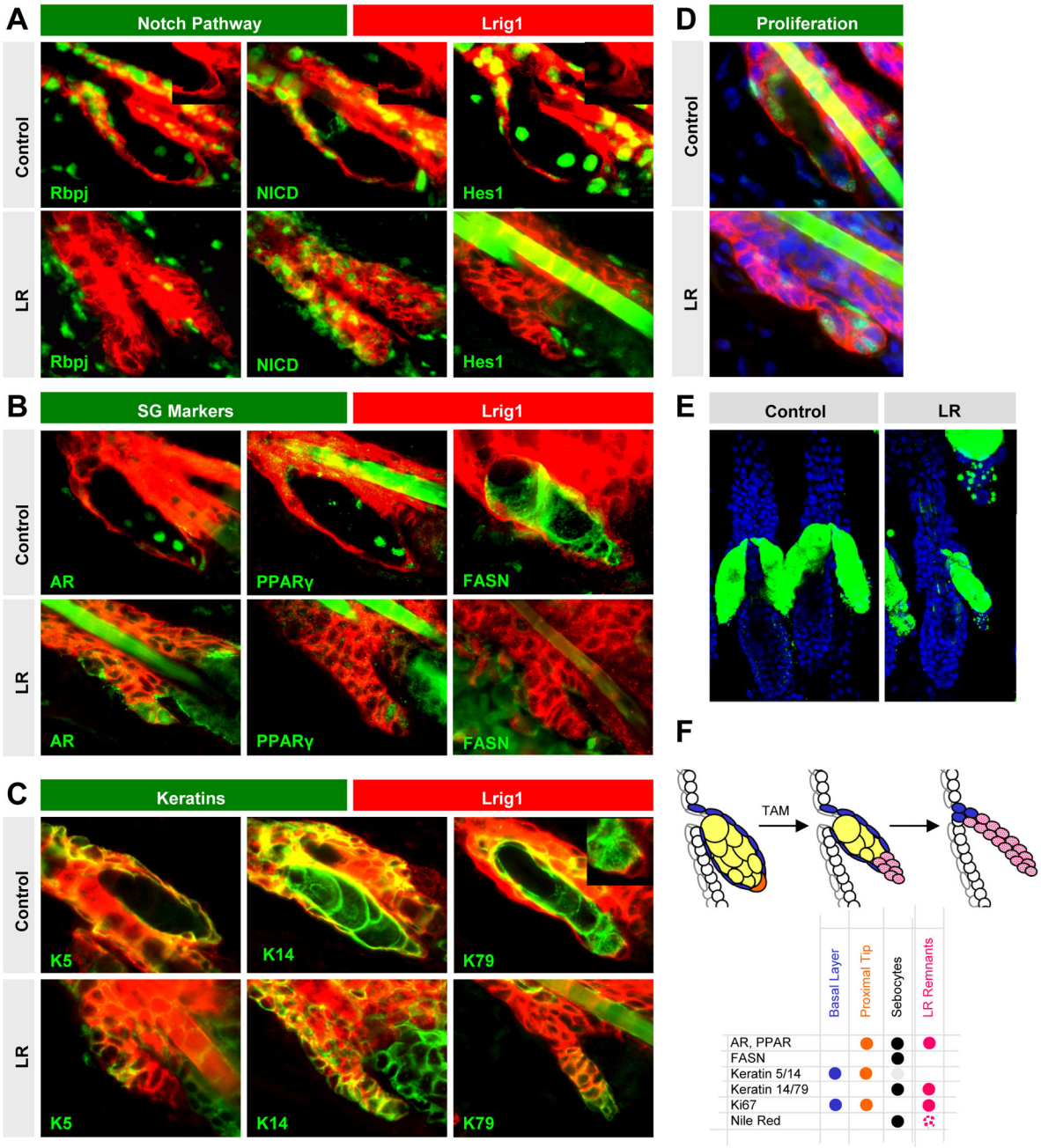

Figure 2. Rbpj promotes SG differentiation.

A. Localization of Notch components (green) in control SGs (upper panels) and LR finger-like remnants (lower panels). Arrow, SG tip. Insets, enhanced single channel views of SG basal layer and tip. NICD, cleaved activated Notch1 intracellular domain. **B.** Same as A, but with SG markers (green). Arrow, SG tip or tip of remnant finger. **C.** Same as A, but with keratin markers (green). **D.** $Ki67^{+}$ cells (green) in control SG basal layer and tip (top arrow), and in LR finger-like remnants (bottom arrow). Red, Lrig1. **E.** WMs showing early lipid accumulation defects originating from the bottom of the LR SG, 2 weeks post-TAM (arrow). **F.** Top, schematic of SG conversion into finger-like remnant in LR follicle. Bottom,

summary. Samples were analyzed 10 weeks post-TAM, unless otherwise noted. Scale bar, 50 μm. See also Figure S2.

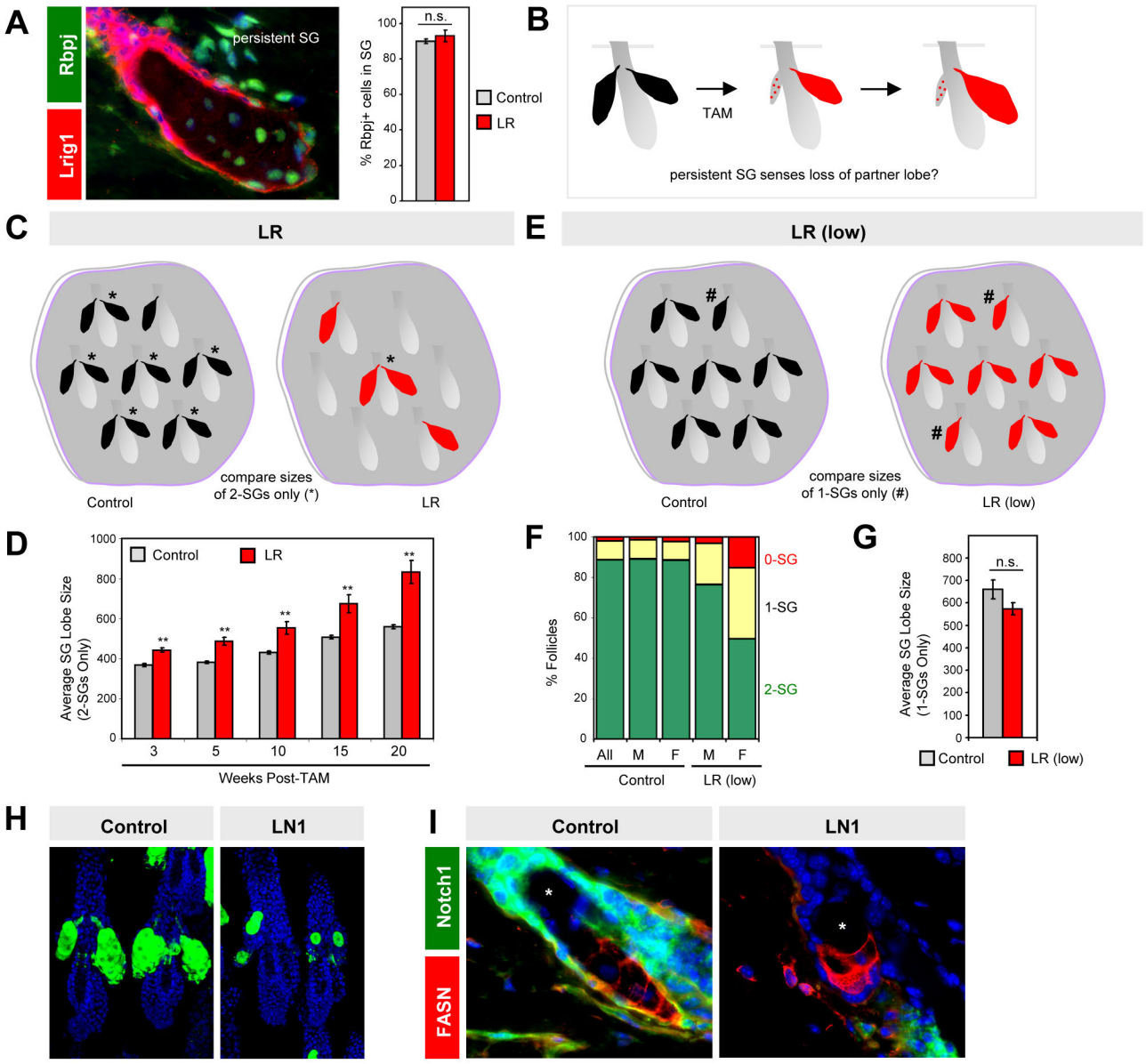

Figure 3. Persistent SGs likely do not enlarge in response to loss of partner lobes.

A. Enlarged persistent SG in LR follicle, 10 weeks post-TAM. Right, quantitation of Rbpj^{+} cells in control SGs and persistent SGs in LR follicles, 10 weeks post-TAM. **B.** Schematic where SG enlarges upon losing its partner lobe. **C.** Schematic where LR 2-SGs (*) are specifically compared with control 2-SGs (*). **D.** Quantitation of SG size for C, by WM. **E.** Schematic where rare 1-SGs (#) in LR-low mice are specifically compared with control 1-SGs (#). **F.** Distribution of follicles with the indicated number of SG lobes, 10 weeks post-TAM. M, males; F, females. **G.** Quantitation of 1-SG size in males by WM, 10 weeks post-TAM. n.s., not significant. **H.** LN1 follicles possess miniaturized SGs. **I.** Miniaturized LN1 SGs express FASN despite losing Notch1. Asterisk, sebaceous duct opening. All SG size measurements were made in pixel units. Data are represented as mean ± SEM. **, $p < 0.01$. Scale bar, 50 μm. See also Figure S3.

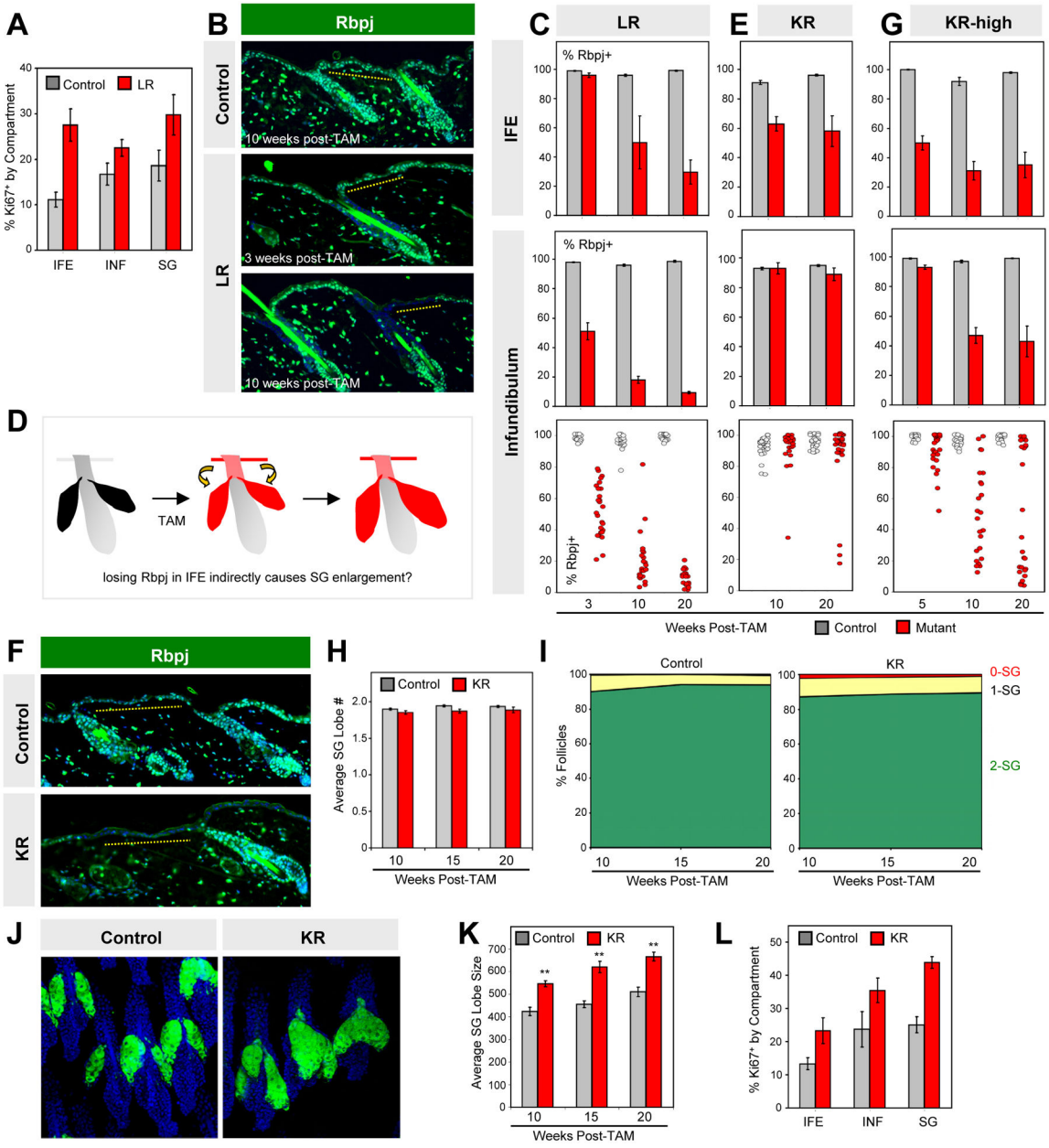

Figure 4. Rbpj indirectly suppresses SGs, likely from the IFE.

A. Ki67 quantitation in different skin compartments, 10 weeks post-TAM. **B.** Histology showing loss of Rbpj in the INF (arrows) and, later, in the IFE (dotted lines) in LR mice. **C.** In LR and control mice, percentage of Rbpj^{+} cells in the IFE (top) and in the INF (middle). Bottom panels, percentage of Rbpj^{+} cells within individual hair follicle infundibula (each circle is a single follicle). **D.** Schematic showing loss of Rbpj in the IFE indirectly causes SG expansion. **E.** Similar to (C), but for KR and control mice. **F.** Staining for Rbpj (green) showing specific deletion in the IFE (dotted lines) but not hair follicle (arrows), in KR skin, 10 weeks post-TAM. **G.** Similar to (C), but for KR-high and control mice. **H.** Quantitation of SG lobe number by WM. **I.** Distribution of follicles with the indicated number of SG lobes. **J.** WM showing enlarged SGs in KR follicles, 10 weeks post-TAM. **K.** Quantitation

of SG size by WM. **L.** Ki67 in different skin compartments, 10 weeks post-TAM. All SG size measurements were made in pixel units. Data are represented as mean ± SEM. **, $p < 0.01$. Scale bar, 50 μm. See also Figure S3-S4.

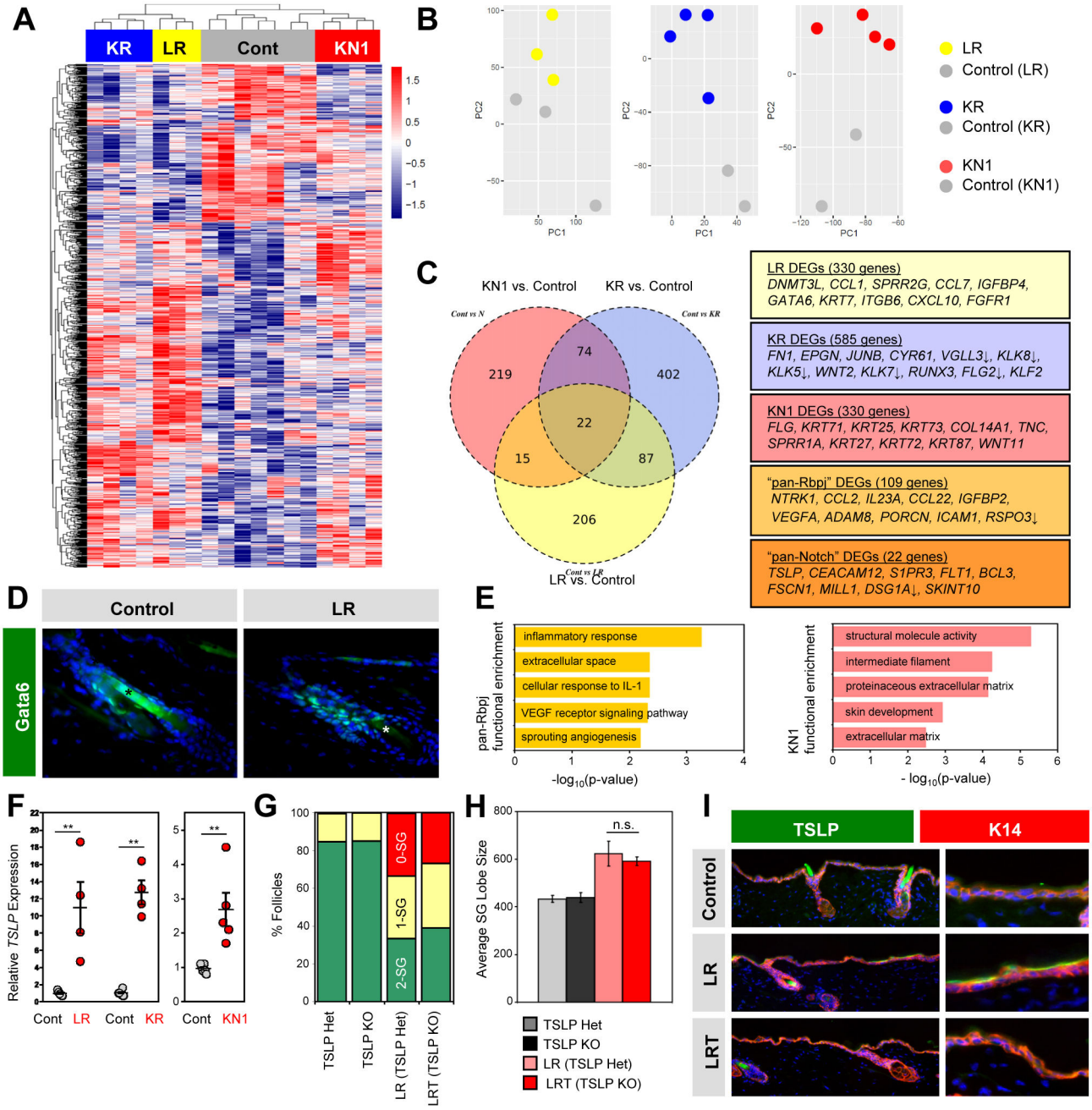

Figure 5. Molecular characterization of Notch deletion.

A. Hierarchical clustering of LR, KR, KN1 and control samples. **B.** Principal component analyses of each set of mutant samples, along with matched controls. **C.** Venn diagram showing overlaps in DEGs when comparing LR, KR and KN1 samples against matched controls. Right panels, notable genes altered in different mutant subsets (FDR ≤ 10% and | $\log_2$fold-change| ≥ 1). ↓, decreased in mutants; all other genes, increased. **D.** LR follicles possess increased Gata6$^+$ cells (arrows). Asterisk, non-specific hair shaft auto-fluorescence. **E.** Enrichment for functional processes altered in both LR and KR samples ("pan-Rbpj," left) or in KN1 samples (right), with notable GO categories labeled. **F.** Validation of

increased *TSLP* in mutants by quantitative RT-PCR. **G.** Distribution of follicles with the indicated SG lobe number by WM, 10 weeks post-TAM. **H.** Loss of TSLP in LRT skin (red) does not prevent SG enlargement, 10 weeks post-TAM. **I.** Confirmation that TSLP (green) is upregulated in LR skin, but absent in LRT skin. n.s., not significant. **, $p < 0.01$. Scale bar, 50 μm. See also Figure S5-S6 and Data S1.

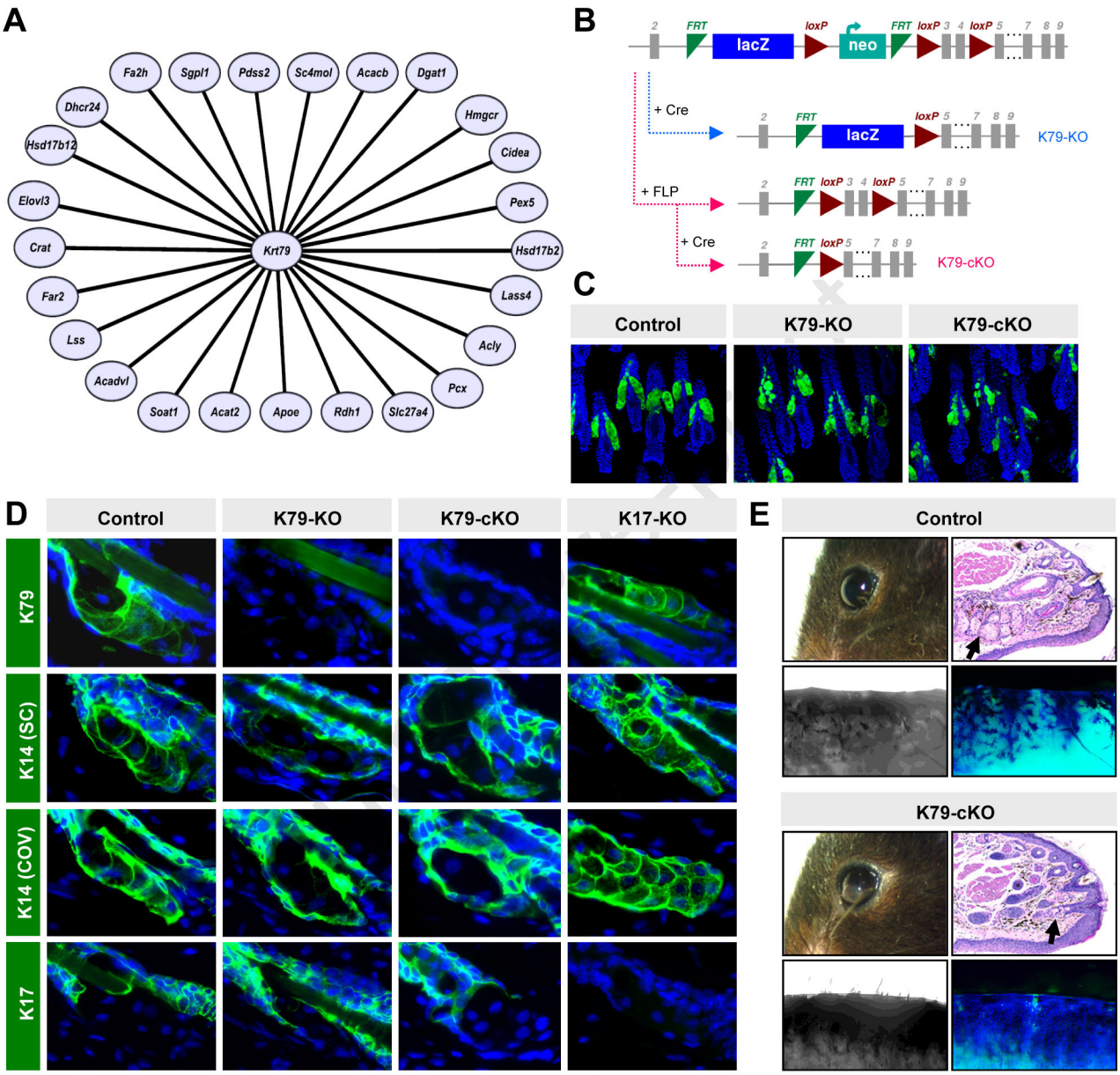

Figure 6. K79 maintains SGs and Meibomian glands.

A. Gene correlation network diagram where nodes indicate genes with expression significantly correlated with *K79* expression (FDR < 0.01, Spearman correlation coefficient > 0.4) and annotated with the Gene Ontology term “lipid metabolic processes” in both of two independent gene expression datasets assaying mouse tail skin (Quigley et al., 2016; Quigley et al., 2009). **B.** Schematic for generating K79-KO and -cKO mice. **C.** WMs of K79-KO and -cKO follicles. **D.** Staining of SGs (dotted lines) for keratin markers (green). Two independent anti-K14 antibodies (SC, COV) were used. Arrows, staining for K14 in control sebocytes, which is absent in K79-KO and -cKO SGs. **E.** Mice lacking K79 (lower) develop corneal lesions (white arrow). Upper right panels, histology of eyelid with black arrows indicating Meibomian glands. Bottom panels, WMs of eyelid illuminated by

brightfield (left) or stained with Nile Red (green) (right) to visualize glands. Scale bar, 50 μm. See also Figure S6 and Data S2.

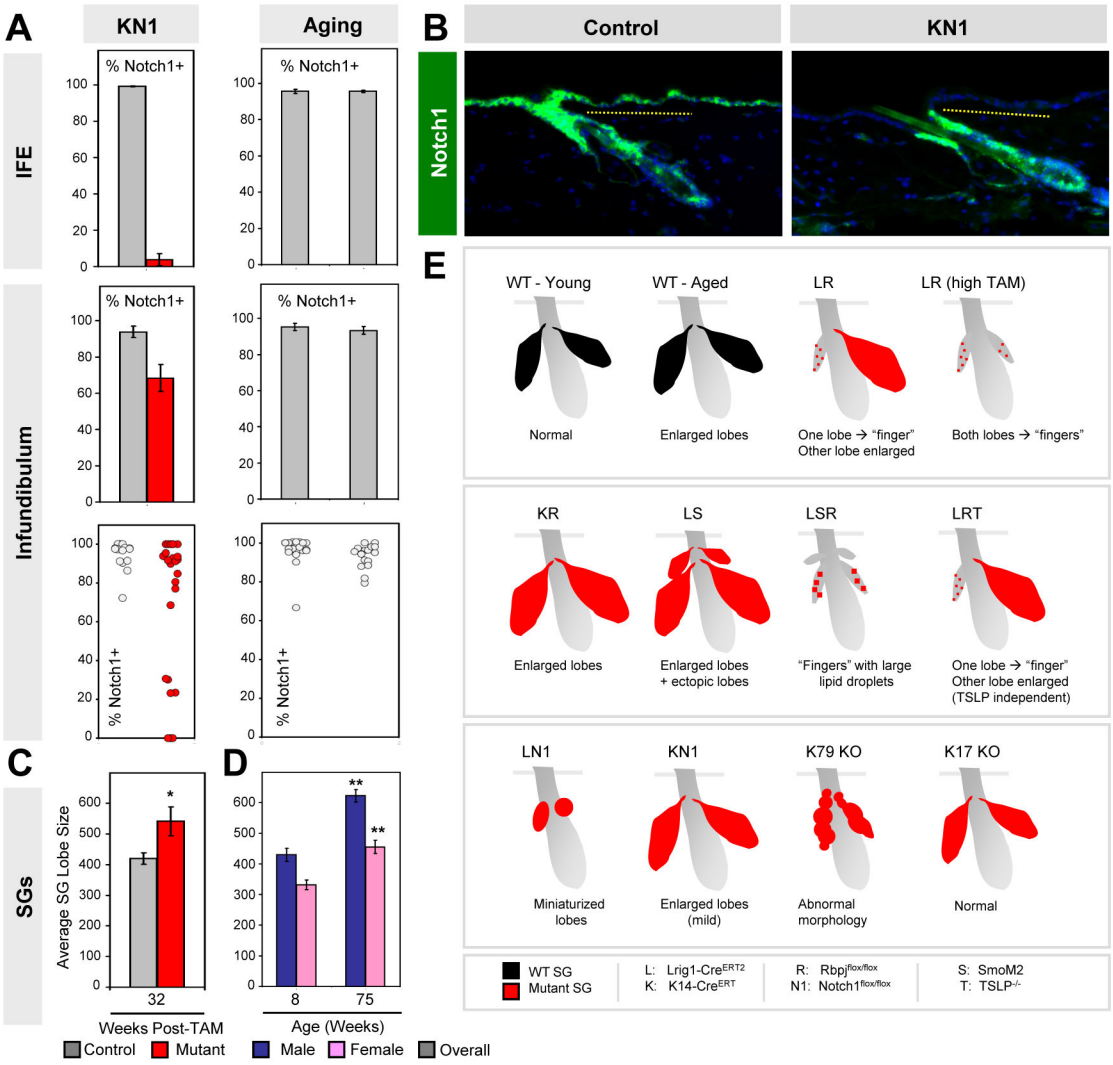

Figure 7. Notch1 indirectly suppresses SGs, likely from the IFE.

A. Percentage of Notch1^{+} cells in the IFE (top) and in the INF (middle). Bottom panel, percentage of Notch1^{+} cells within individual hair follicle infundibula (each circle is a single follicle). **B.** Histological staining for Notch1 (green) showing specific deletion in the IFE (dotted lines), but not hair follicle (arrow), in KN1 skin, 32 weeks post-TAM. **C.** SG lobe size in KN1 and control mice. **D.** SG lobe size in young and aged mice. **E.** Summary of SG phenotypes described in this study. All SG size measurements were made in pixel units. Data are represented as mean ± SEM. *, $p < 0.05$; **, $p < 0.01$. Scale bar, 50 μm. See also Figure S7.

KEY RESOURCES TABLE

REAGENT or RESOURCE	SOURCE	IDENTIFIER
Antibodies		
Rabbit anti-androgen receptor	Santa Cruz	Cat # sc-816
Rabbit anti-cleaved caspase-3	Cell Signaling	Cat # 9661
Mouse anti-FASN	BD	Cat # 610963
Rabbit anti-Gata6	Cell Signaling	Cat # D61E4
Chicken anti-GFP	Aves Labs	Cat # GFP-1010
Rabbit anti-Hes1	Cell Signaling	Cat # 11988S
Rabbit anti-Ki67	Cell Signaling	Cat # 12202S
Guinea Pig anti-K5	American Research Products	Cat # 03-GP-CK5
Goat anti-K14	Santa Cruz (SC)	Cat # sc-17104
Rabbit anti-K14	Covance (COV)	Cat # PRB-155P
Rabbit anti-K17	Coulombe Lab	N/A
Goat anti-K79	Santa Cruz	Cat # sc-243156
Rabbit anti-K79 (NOTE: see Veniaminova et al., 2013)	Abcam	Cat # Ab7195
Goat anti-Lrig1	R&D Systems	Cat # AF3688-SP
Rabbit anti-NICD	Cell Signaling	Cat # 4147P
Rabbit anti-Notch1	Cell Signaling	Cat # 3608S
Rabbit anti-PPARy	Santa Cruz	Cat # sc-7196
Rabbit anti-Rbpj	Cell Signaling	Cat # 5313P
Goat anti-Tslp	R&D Systems	Cat # AF555-SP
Biological Samples		
Mouse skin samples, obtained in accordance with guidelines established by the University of Michigan Unit for Laboratory Animal Medicine	This manuscript	Study protocol # PRO00008196
Chemicals, Peptides, and Recombinant Proteins		
Tamoxifen	Sigma	Cat # T5648
TSA Fluorescein Plus kit	Perkin Elmer	Cat # NEL741E001KT
Nile Red	Sigma	Cat # N3013
RNeasy Mini Kit	Qiagen	Cat # 74104
Deposited Data		
RNA-seq data	This manuscript	GEO: GSE125737
Experimental Models: Organisms/Strains		
Mouse: Lrig1$^{tm1.1(cre/ERT2)Rjc}$ (Lrig1-Cre^{ERT2})	Powell et al., 2012; The Jackson Laboratory	Cat # 018418
Mouse: Tg(KRT14-cre/ERT)20Efu/J (K14-Cre^{ERT})	Vasioukhin et al., 1999; The Jackson Laboratory	Cat # 005107
Mouse: Rbpj^{tm1Hon} (Rbp-j^{flox})	Yamamoto et al., 2003; Laboratory of Dr. Tasuku Honjo	MGI:3583755
Mouse: Notch1^{tm2Rko}/GridJ (Notch1^{flox})	Yang et al., 2004; The Jackson Laboratory	Cat # 007181

REAGENT or RESOURCE	SOURCE	IDENTIFIER
Mouse: Gt(ROSA)26Sor$^{tm1(Smo/EYFP)Amc}$/J (SmoM2)	Mao et al., 2006; The Jackson Laboratory	Cat # 005130
Mouse: Krt79$^{tm2b(KOMP)Wtsi}$ (K79-KO)	Mesler et al., 2017; Laboratory of Dr. Sunny Wong	N/A
Mouse: Krt79$^{tm2c(KOMP)Wtsi}$ (K79-cKO)	This manuscript	N/A
Mouse: Krt17^{tm1Cou} (K17-KO)	McGowan et al., 2002; Laboratory of Dr. Pierre Coulombe	MGI:2651542
Mouse: Tslp^{tm1Sfz} (TSLP-KO)	Han et al., 2012; Laboratory of Dr. Steve Ziegler	MGI:5503051
Mouse: Tg(KRT5-cre)5132Jlj (K5-Cre)	Ramirez et al., 2004; Laboratory of Dr. Anj Dlugosz	MGI:3050065
Oligonucleotides		
qPCR primer: TSLP-For: 5’-CCAGGCTACCCTGAAACTGA-3’	This manuscript	N/A
qPCR primer: TSLP-Rev: 5’-TCTGGAGATTGCATGAAGGA-3’	This manuscript	N/A
Software and Algorithms		
Prism, Version 6	GraphPad	https://www.graphpad.com/scientific-software/prism/
AxioVision, Version 4	Carl Zeiss	https://www.zeiss.com/microscopy/us/products/microscope-software/axiovision.html
HTSeq (GENCODE v18 gene model)	Anders et al., 2015	https://htseq.readthedocs.io/en/release_0.11.1/
DESeq2	Bioconductor	https://bioconductor.org/packages/release/bioc/html/DESeq2.html
DAVID	Huang et al., 2009	https://david.ncifcrf.gov/
BiNGO	Maere et al., 2005	https://www.psb.ugent.be/cbd/papers/BiNGO/Home.html
Cytoscape	Shannon et al., 2003	https://cytoscape.org
Other		